

AT 15 1956

Copy 5
RM L56H07

NACA RM L56H07

C1

UNCLASSIFIED



RESEARCH MEMORANDUM

AN EXPERIMENTAL STUDY OF THE
ZERO-ANGLE-OF-ATTACK TRANSONIC DRAG ASSOCIATED
WITH THE VERTICAL POSITION OF A HORIZONTAL
TAIL AT ZERO INCIDENCE

By Robert R. Howell✓

Langley Aeronautical Laboratory
Langley Field, Va.

UNCLASSIFIED

LIBRARY COPY

To

OCT 30 1956

By authority of

NASA

PA-1 Effort

LANGLEY AERONAUTICAL LABORATORY
LIBRARY NACA
LANGLEY FIELD, VIRGINIA

CLASSIFIED DOCUMENT 9/17/58
This material contains information affecting the National Defense of the United States within the meaning of the espionage laws, Title 18, U.S.C., Secs. 793 and 794, the transmission or revelation of which in any manner to an unauthorized person is prohibited by law.

**NATIONAL ADVISORY COMMITTEE
FOR AERONAUTICS**

WASHINGTON

October 25, 1956

UNCLASSIFIED

NATIONAL ADVISORY COMMITTEE FOR AERONAUTICS

RESEARCH MEMORANDUM

AN EXPERIMENTAL STUDY OF THE
ZERO-ANGLE-OF-ATTACK TRANSONIC DRAG ASSOCIATED
WITH THE VERTICAL POSITION OF A HORIZONTAL
TAIL AT ZERO INCIDENCE

By Robert R. Howell

SUMMARY

An experimental study has been made of the transonic drag associated with varying the vertical location of the horizontal tail of a representative tail-body combination. The tail had zero incidence. Factors which significantly influenced the results were flow separation in the horizontal tail-body juncture, afterbody-tail-interference pressure drag, and a downwash over the horizontal tail which resulted from the boundary conditions of the converging afterbody. Inasmuch as these factors are present, the calculation of the empennage drag by use of area-development methods may possibly be subject to large errors in cases where the horizontal and vertical tails are located near but not in the planes of symmetry.

INTRODUCTION

The problem of determining the transonic-drag increment due to the empennage of an airplane has become increasingly important. Modern methods of predicting the pressure drag of smooth slender bodies on the basis of longitudinal area developments, such as reference 1, may not be readily adaptable to the problem of determining a quantitative value for the empennage drag because of the large local effects which are believed to be present for most empennage designs. It is the purpose of the present paper to present the results of an experimental investigation which was made to explore the effect of vertical position of a fixed horizontal stabilizer on the zero-angle-of-attack transonic drag of a tail-body combination and to determine, if possible, some of the major sources of empennage drag.

████████████████████

The investigation was carried out in the Langley transonic blowdown tunnel. The tests, which covered a range of Mach number from 0.72 to 1.28, were made at a Reynolds number of approximately 10×10^6 based on model length.

SYMBOLS

| | |
|---------------|--|
| A_b | area of model base, sq in. |
| C_{D_T} | total-drag coefficient, $\frac{\text{Measured drag}}{q_o F}$ |
| C_{D_b} | base-drag coefficient, $-\frac{(p_b - p_o) A_b}{q_o F}$ |
| $C_{D_{ext}}$ | external-drag coefficient, $C_{D_T} - C_{D_b}$ |
| c | local chord |
| F | maximum frontal area of model, 0.785 sq in. |
| P | pressure coefficient, $\frac{p - p_o}{q_o}$ |
| p_b | measured base pressure |
| p_o | free-stream static pressure |
| M_o | free-stream Mach number |
| L | total body length |
| q_o | free-stream dynamic pressure, $0.7 p_o M_o^2$ |
| x | longitudinal distance |
| r | body radius |

MODELS

A photograph of the model and the different empennage configurations tested is presented in figure 1. A sketch of the model including pertinent dimensions is presented in figure 2. The body was composed of a parabolic nose with a fineness ratio of 4.0, a cylindrical center section, and a parabolic afterbody with a fineness ratio of 2.0. All of the configurations were constructed of brass. Nondimensional design ordinates for the model fuselage are presented in table I. The four empennage configurations investigated were obtained by changing the vertical location of the horizontal tail only. The components of the empennage and the other locating dimensions remained fixed. The four vertical locations of the horizontal tail corresponded to distances of 0, 1, 2, and 3 base radii above the model center line. The horizontal tail, which had an aspect ratio of 3.57, a taper ratio of 0.3, a sweepback of the quarter chord of 45° , and NACA 65A007 airfoil sections parallel to the stream direction, was fixed at 0° incidence. The vertical tail had the same geometric characteristics as the horizontal tail. The cross-sectional-area development of the five configurations tested is presented in figure 3.

APPARATUS

The tests were conducted in the Langley transonic blowdown tunnel. This tunnel has an octagonal, slotted test section measuring 26 inches between flats. The model was attached to an internal axial-force electric strain-gage balance which was sting supported in the tunnel. (See fig. 2.) The angle of attack of the model was carefully set at zero with a sensitive inclinometer.

The pressure acting on the model base was measured by means of inserting an open-end tube through the sting and into an open section of the strain-gage balance. The pressure so measured was the average pressure acting on the open area of the base.

Force data were recorded by photographing a self-balancing potentiometer. The base-pressure data were photographically recorded simultaneously with the force measurements by a quick-response flight-type recorder. An indication of the accuracy of the measurements may be obtained by consideration of the scatter of data points presented.

TESTS

Zero-angle-of-attack drag of the body alone and the body in combination with four tail configurations was determined through a range of Mach number between 0.72 and 1.28. The Reynolds number based on body length varied between 9.7×10^6 and 11.5×10^6 as indicated in figure 4. Schlieren observations indicated that the tunnel-wall reflected disturbances interfered with the model in the Mach number range between about 1.04 and 1.13. No data are presented for this Mach number range.

The tests were made with a 1/16-inch-wide strip of carborundum particles running spanwise and located on both surfaces of the tails at 10 percent of the local chord behind the leading edge. The 0.001-inch-diameter particles were blown on a wet strip of thinned shellac. There was also a similarly constructed 1/4-inch-wide band of roughness around the forebody of the fuselage located 1 inch back of the nose. Care was taken to insure that the roughness strips were generally the same for all of the tail configurations.

During the testing, some oil-flow studies and some schlieren observations and photographs were made to indicate the nature of the flow around the empennage of the configurations.

RESULTS AND DISCUSSION

The total-, base-, and external-drag coefficients of the different tail configurations as determined by the tests are presented in figure 5. A comparison of the variation of external-drag coefficient with Mach number for the different configurations is made in figure 6. Also presented for comparison in figure 6 are the viscous drag coefficients at $M_0 = 0.8$ of the body alone and the body plus tail as calculated on the basis of fully turbulent flow and equivalent flat-plate area (ref. 2). Inasmuch as the model was tested at zero angle of attack rather than at zero pitch, the quantitative values of drag coefficient presented do not in all cases correspond to the trimmed condition.

The variation in subsonic-drag-coefficient level with changes in horizontal-tail position, as indicated in figure 6, is believed to result from a number of factors. Oil-flow studies made at $M_0 = 0.93$ (fig. 7) showed that one of the factors was a varying extent of flow separation in the tail-body juncture with varying vertical position of the horizontal tail. The configuration with the horizontal tail on the body center line (designated tail 1) had no apparent flow separation. As the horizontal tail was moved progressively away from the fuselage

center line (tails 2, 3, and 4), the extent of the separated region increased. At the most outward position tested (tail 4), there was evidence of flow separation on both the lower surface of the horizontal tail and on the adjacent surface of the body. Schlieren observations indicated that regions of supersonic flow surrounded the model afterbody for Mach numbers as low as 0.85. (See the schlieren photographs at $M_0 = 0.93$ in fig. 8, for example.) The observation of supersonic flow and discrete waves near the afterbody at these subsonic speeds suggests that another possible factor influencing the subsonic-drag-coefficient level is the change in interference pressure drag with a change in the vertical position of the horizontal tail. That this may be true is suggested by the fact that there are differences in base-pressure drags. (See, for example, tail 3 in fig. 5.) Some of these interference effects may be favorable. This favorable effect, of course, may account for the tail 1 configuration having a subsonic level slightly lower than that estimated on the basis of viscous-drag calculations (fig. 6). Yet, another factor having a significant influence on the subsonic-drag increment due to the tail is the downwash imposed on the horizontal-tail surface as a result of boattailing the fuselage afterbody. Although the exact magnitude of the effects at subsonic speeds due to the downwash is not known, it should be recognized that such an effect is a factor influencing the drag of any configuration having a converging afterbody and a horizontal stabilizer which is located near but off the body center line.

In addition to the noted variations in the subsonic-drag-coefficient levels, there were also differences in the supersonic pressure drag rise (fig. 6). These results are substantiated to a large degree by unpublished results obtained from a similar investigation made in free flight. An explanation for some of the differences in supersonic pressure drag rises is that the factors which influenced the drag at subsonic speeds persisted into the supersonic speed range. The regions of flow separation, though small, were still present at $M_0 = 1.24$ (fig. 7). The variation in base-pressure drag with vertical location of the horizontal tail also still persisted at supersonic speeds (fig. 5), thus indicating variations in afterbody pressure drag. Schlieren observations at a Mach number of 1.24 (fig. 8) showed that, in addition to changes in the flow field with a change in horizontal-tail location, there was a gradual deflection of the model support as the tail was moved away from the body center line. This result was not indicated at $M_0 = 0.93$. Apparently, there was a decided increase in the down load on the horizontal tail as the Mach number became supersonic. A down load on the tail is reflected as a reduction in pressure over the boattailed afterbody due to the reduced pressures on the lower surface of the tail which, of course, corresponds to a drag force. Checks made to determine whether such a deflection might cause erroneous measurements as a result of strain-gage interaction or small differences in model angle of attack indicated that the possible errors in drag coefficient could be no more than that indicated by the scatter of data points.

~~CONFIDENTIAL~~

In order to obtain an indication of the effective downwash due to the presence of the boattailed afterbody, a computation was made of the mean downwash angle in the region of the most outward position of the horizontal tail. The most outward position (tail 4) was chosen since it was indicated to have the greatest effective downwash of the four empennage configurations tested. The angle was computed by first determining the slope of the streamlines relative to the body axis in an assumed axisymmetric field around the body, and then by integrating the component of this slope in the plane normal to the chord plane along the 50-percent-chord line of the horizontal tail. The calculations were made on the basis of slender-body approximations for a Mach number of 1.2. The calculated mean downwash angle amounted to about 4.25° . An estimation was also made of the pressure distribution that would exist over the body surface at $M_0 = 1.2$ if the tail were not present (fig. 9). It was indicated that at supersonic speeds there was, in addition to the significant downwash angle, a decrease in local static pressure or an increase in dynamic pressure in the region of the tail of this configuration. It is most likely that a combination of the downwash angle and the local increase in dynamic pressure caused the indicated download on the tail. It should be pointed out that down loading on the horizontal tail, such as that just discussed in connection with the boattailed afterbody, is more generally obtained in satisfying the trim conditions for a complete airplane in flight. The magnitude of this interference drag resulting from the tail load required for trim will, of course, also depend upon the vertical position of the horizontal tail in the same manner as indicated in the present investigation for the afterbody-induced tail loads.

It becomes evident from considering these possible drag sources (that is, drag due to local interference and separation, and drag resulting from loads on the horizontal tail) that one should avoid attempts to compute the absolute drag of empennage configurations such as those tested in the present investigation on the basis of area development alone. The area rule is not intended to be applicable where such local flow phenomena exist.

CONCLUDING REMARKS

It has been demonstrated by wind-tunnel tests that the transonic zero angle-of-attack drag of a representative zero-incidence tail-body combination is significantly dependent upon the vertical location of the horizontal tail. Horizontal-tail locations nearest the plane of symmetry afforded the lowest drags. Factors which significantly influenced the results were flow separation in the horizontal-tail-body juncture, afterbody-tail-interference pressure drag, and a downwash over the horizontal tail which resulted from the boundary conditions of the converging

afterbody. Inasmuch as these factors are present, the calculation of the empennage drag by use of area-development methods may possibly be subject to large errors in cases where the horizontal and vertical tails are located near but not in the planes of symmetry.

Langley Aeronautical Laboratory,
National Advisory Committee for Aeronautics,
Langley Field, Va., July 26, 1956.

REFERENCES

1. Holdaway, George H.: Comparison of Theoretical and Experimental Zero-Lift Drag-Rise Characteristics of Wing-Body-Tail Combinations Near the Speed of Sound. NACA RM A53H17, 1953.
2. Rubesin, Morris W., Maydew, Randall C., and Varga, Steven A.: An Analytical and Experimental Investigation of the Skin Friction of the Turbulent Boundary Layer on a Flat Plate at Supersonic Speeds. NACA TN 2305, 1951.

TABLE I
NONDIMENSIONAL DESIGN ORDINATES OF BODY

| x/L | r/L |
|--------|-------|
| 0 | 0 |
| .0357 | .0085 |
| .0714 | .0162 |
| .1071 | .0232 |
| .1429 | .0294 |
| .1786 | .0347 |
| .2143 | .0392 |
| .2500 | .0429 |
| .2857 | .0459 |
| .3214 | .0480 |
| .3571 | .0494 |
| .3929 | .0499 |
| .4000 | .0500 |
| .8000 | .0500 |
| .8214 | .0497 |
| .8571 | .0479 |
| .8929 | .0446 |
| .9286 | .0396 |
| .9643 | .0323 |
| 1.0000 | .0249 |

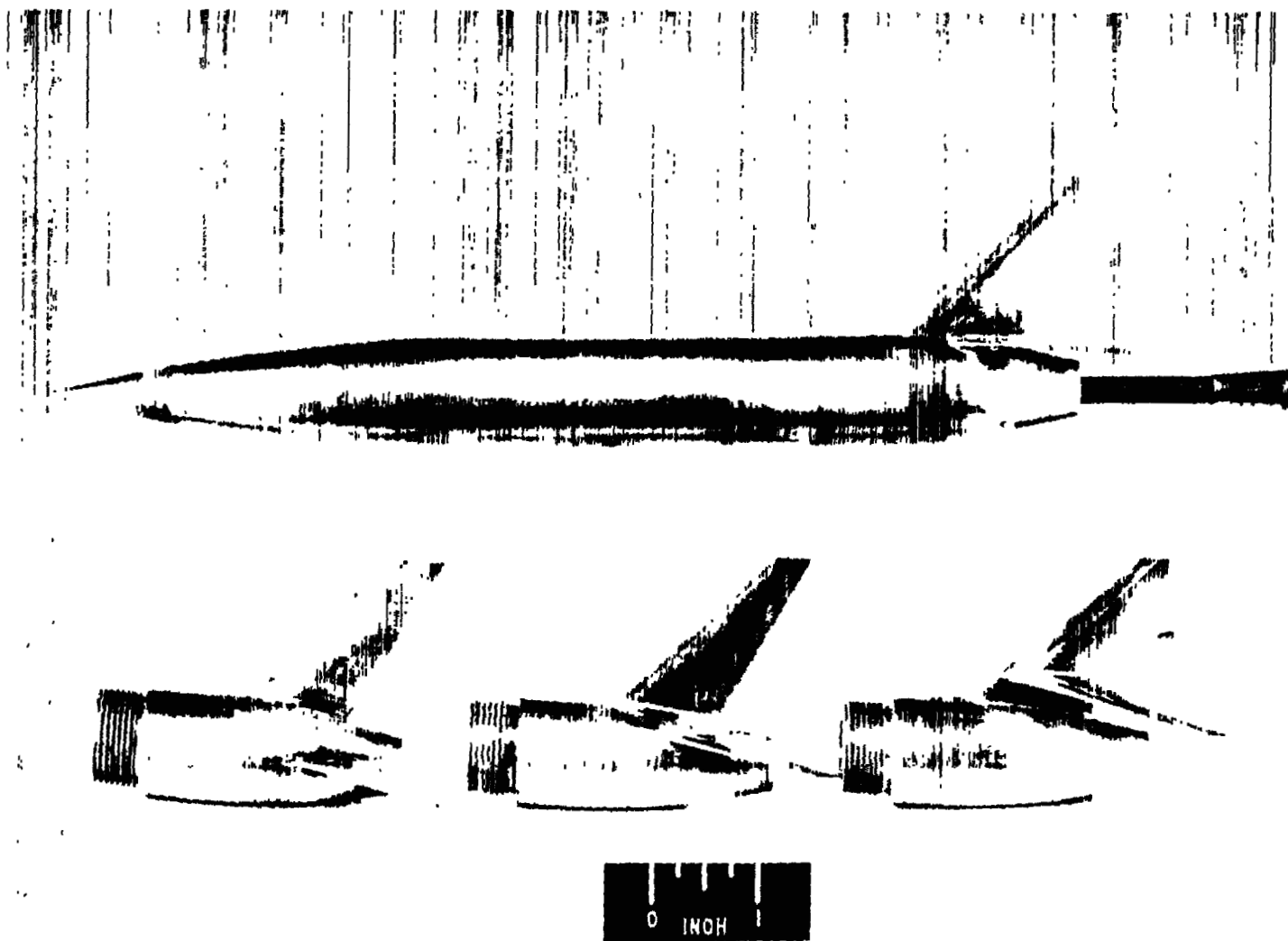


Figure 1.- Photograph of model and different tail configurations tested.

L-90269

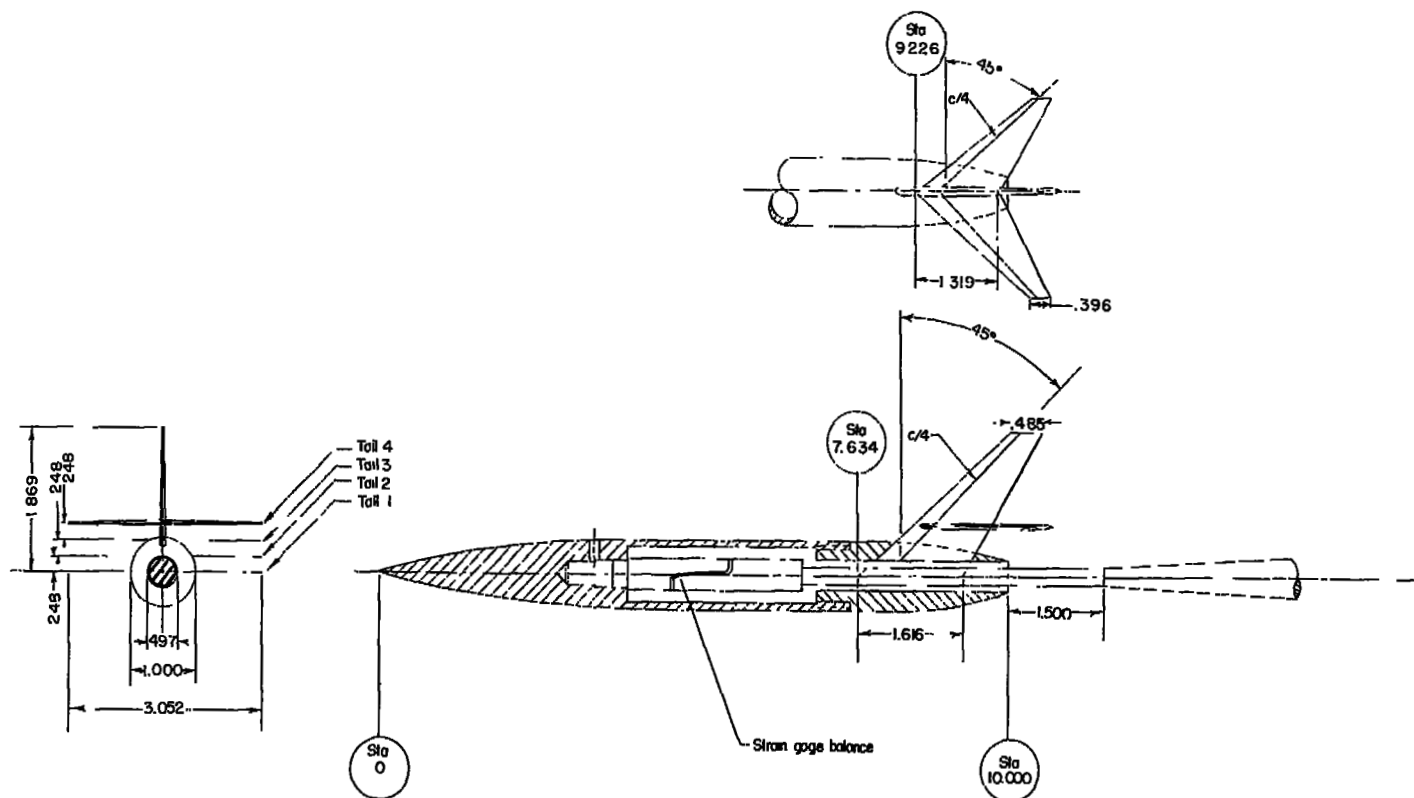


Figure 2.- Sketches showing details and pertinent dimensions of the tail-fuselage combinations tested. All dimensions are in inches.

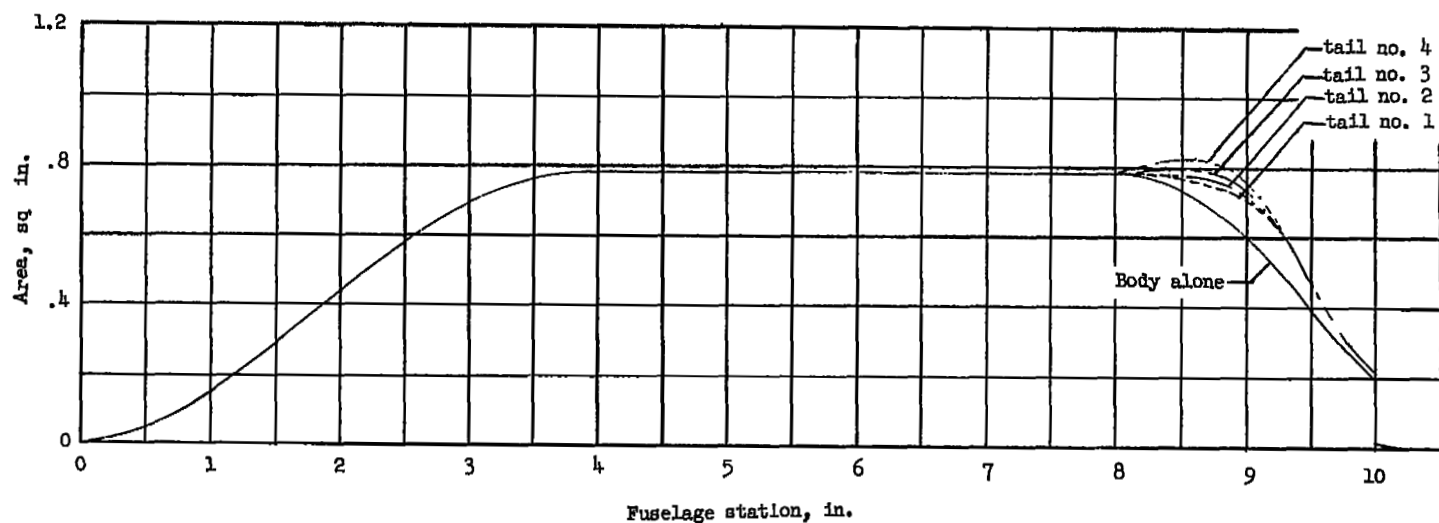


Figure 3.- The longitudinal development of cross-sectional area of the configurations with and without tails.

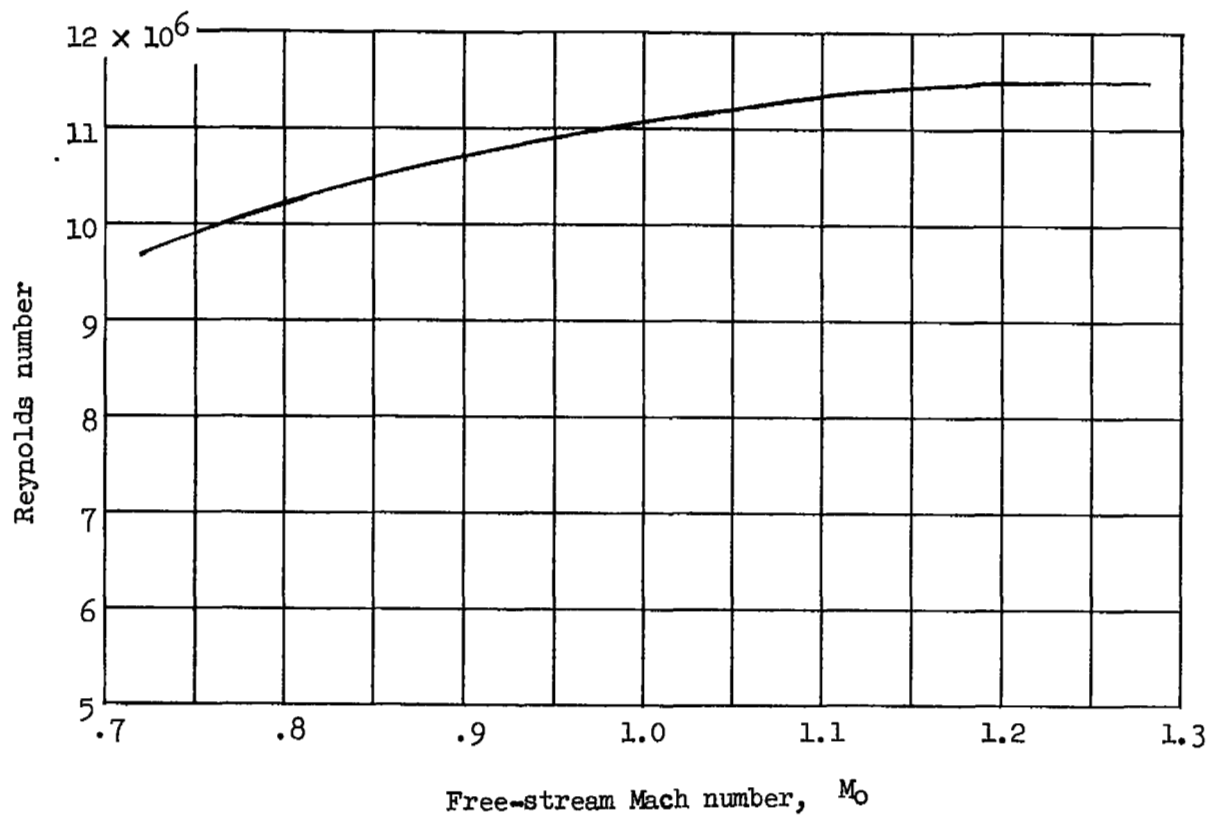
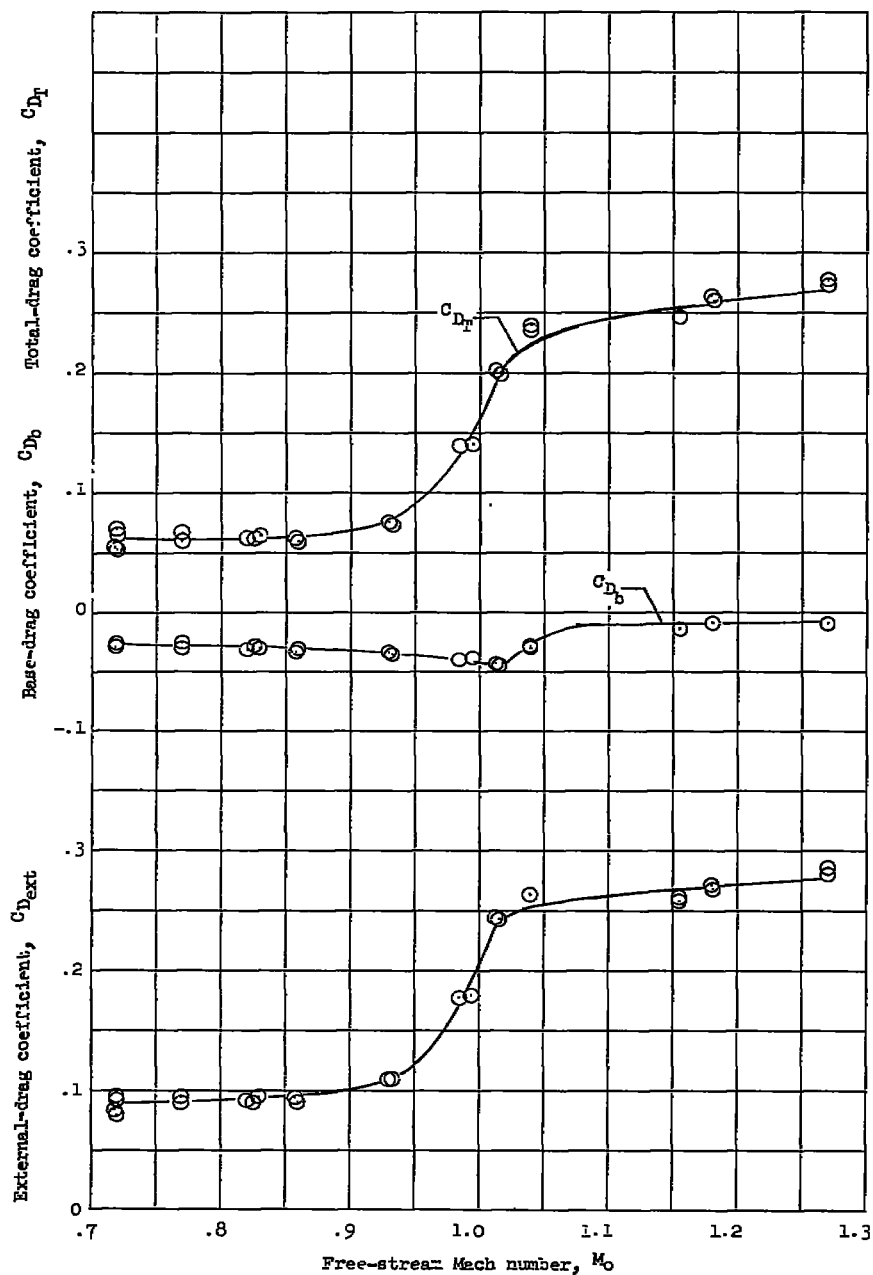
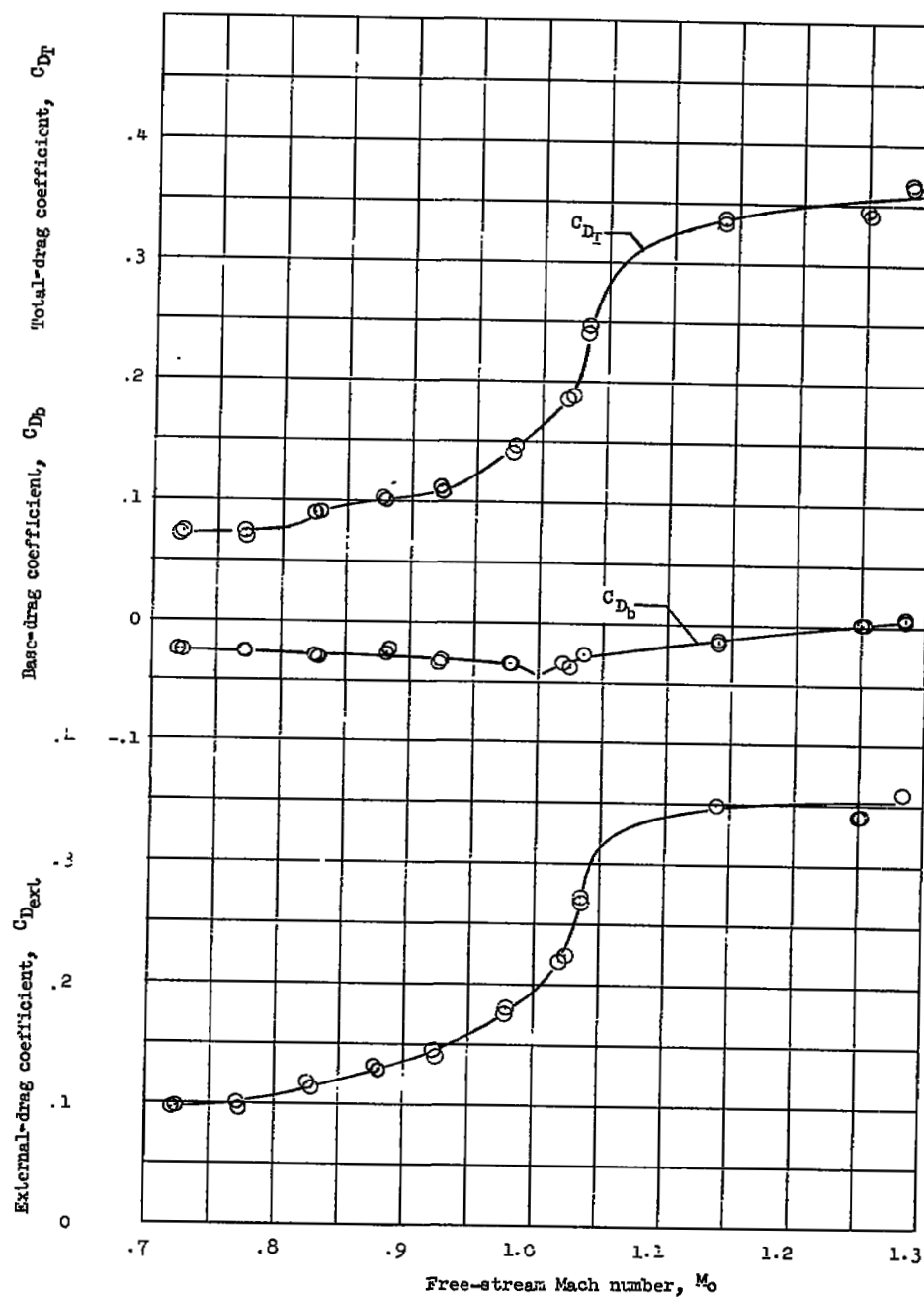


Figure 4.- The variation with Mach number of the test Reynolds number based on model length.



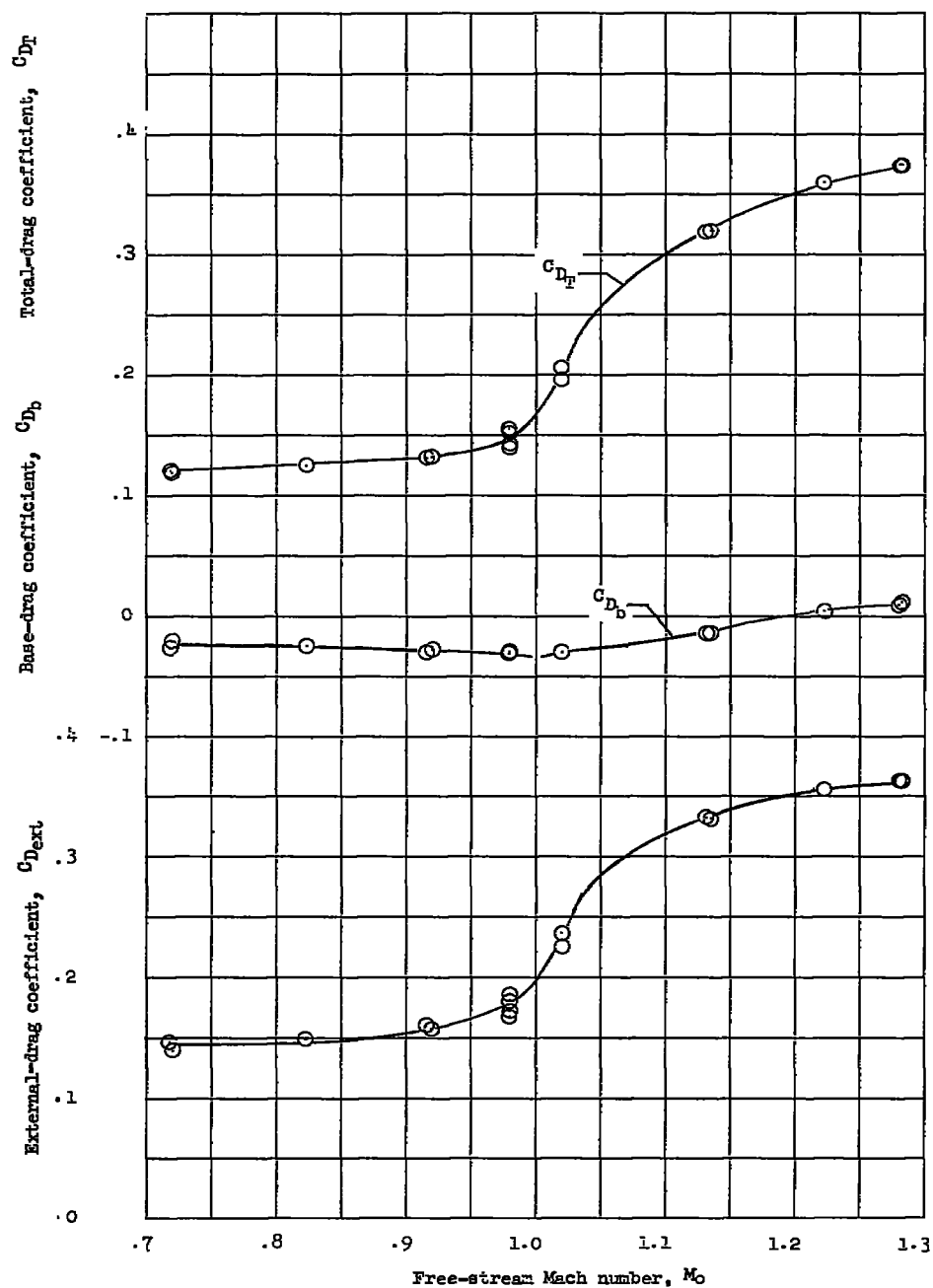
(a) Body alone.

Figure 5.- The variation in total-, base-, and external-drag coefficient with Mach number for the various tail configurations as determined by wind-tunnel tests.



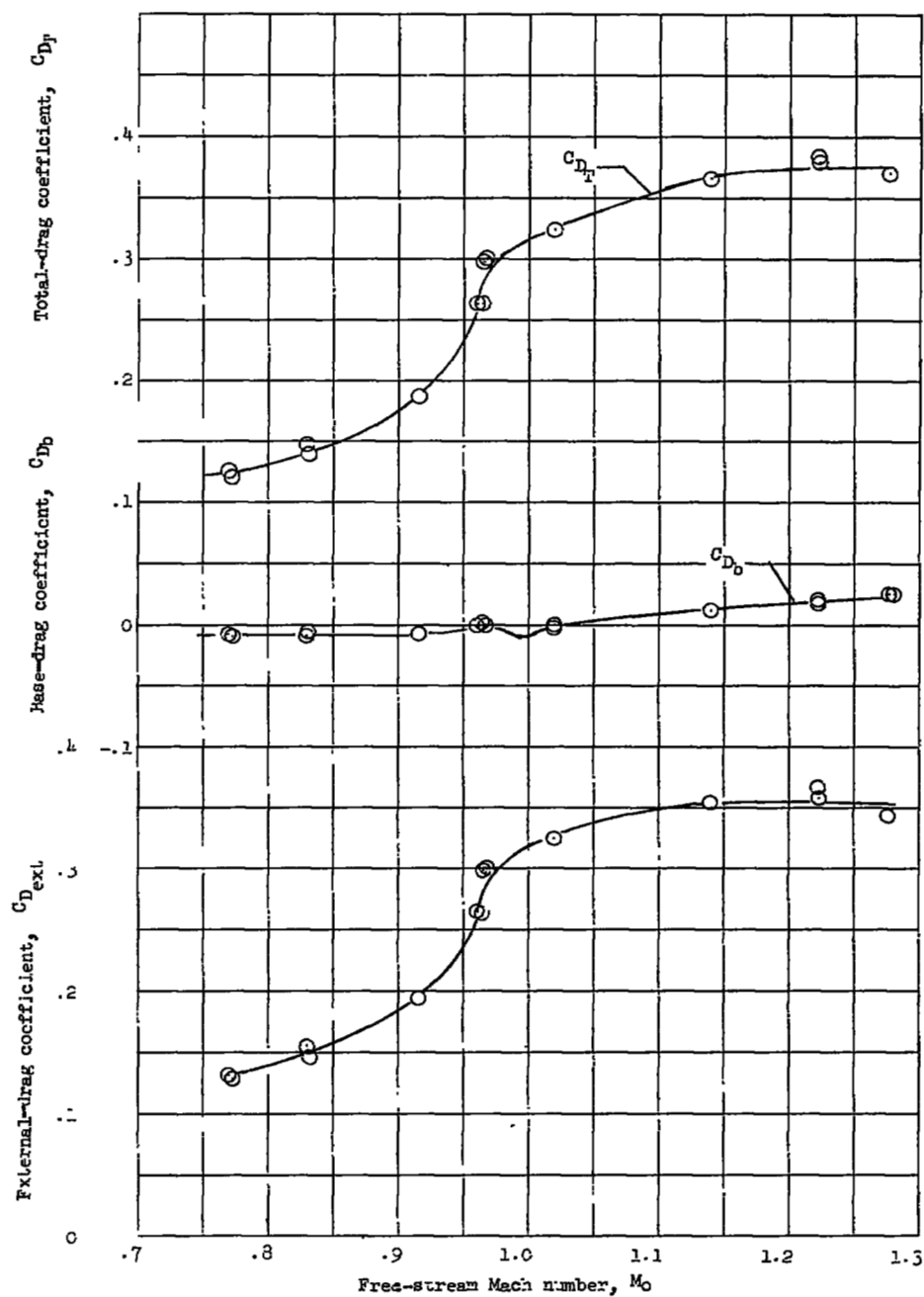
(b) Tail 1.

Figure 5.- Continued.



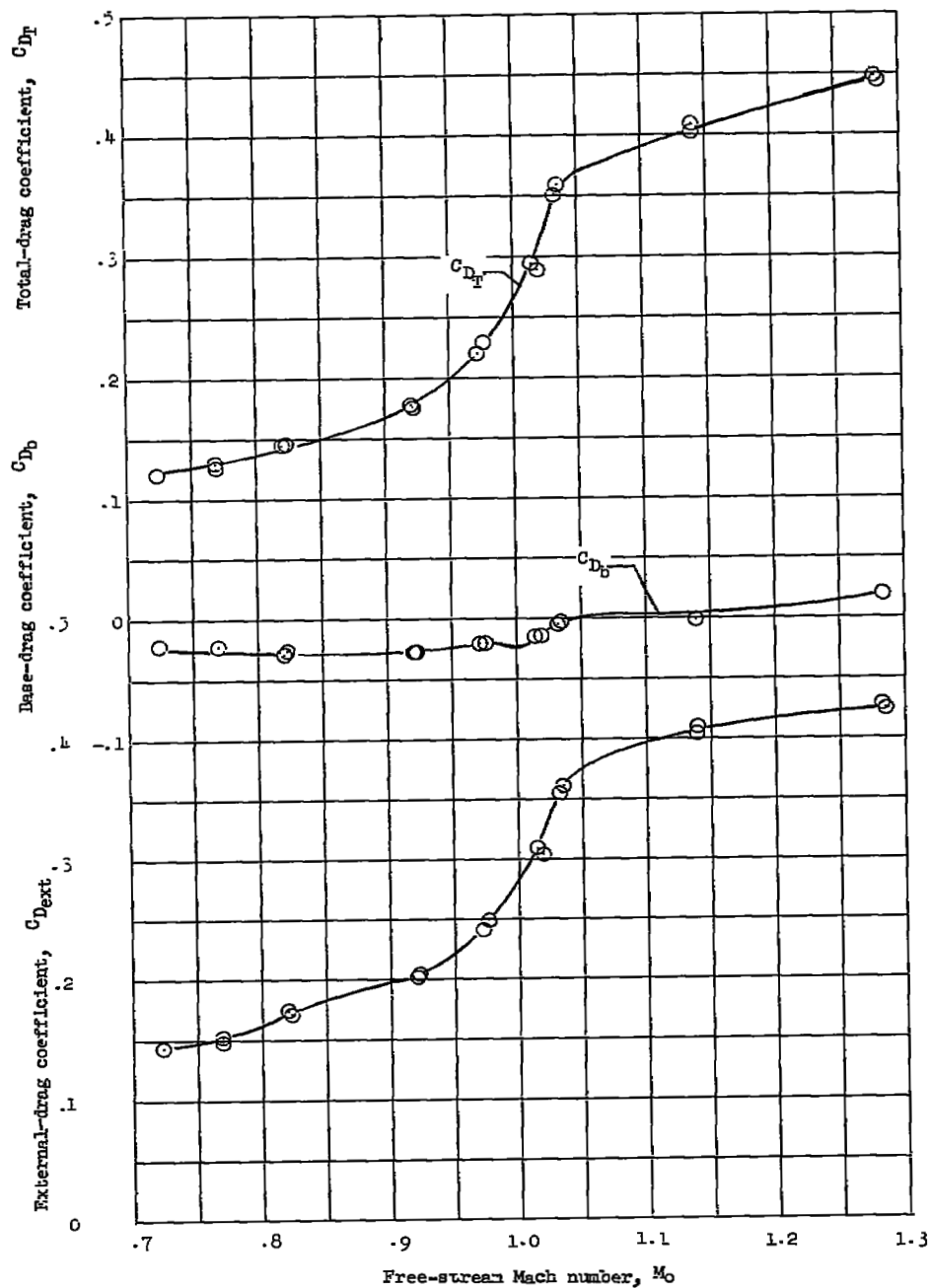
(c) Tail 2.

Figure 5.- Continued.



(d) Tail 3.

Figure 5.- Continued.



(e) Tail 4.

Figure 5.- Concluded.

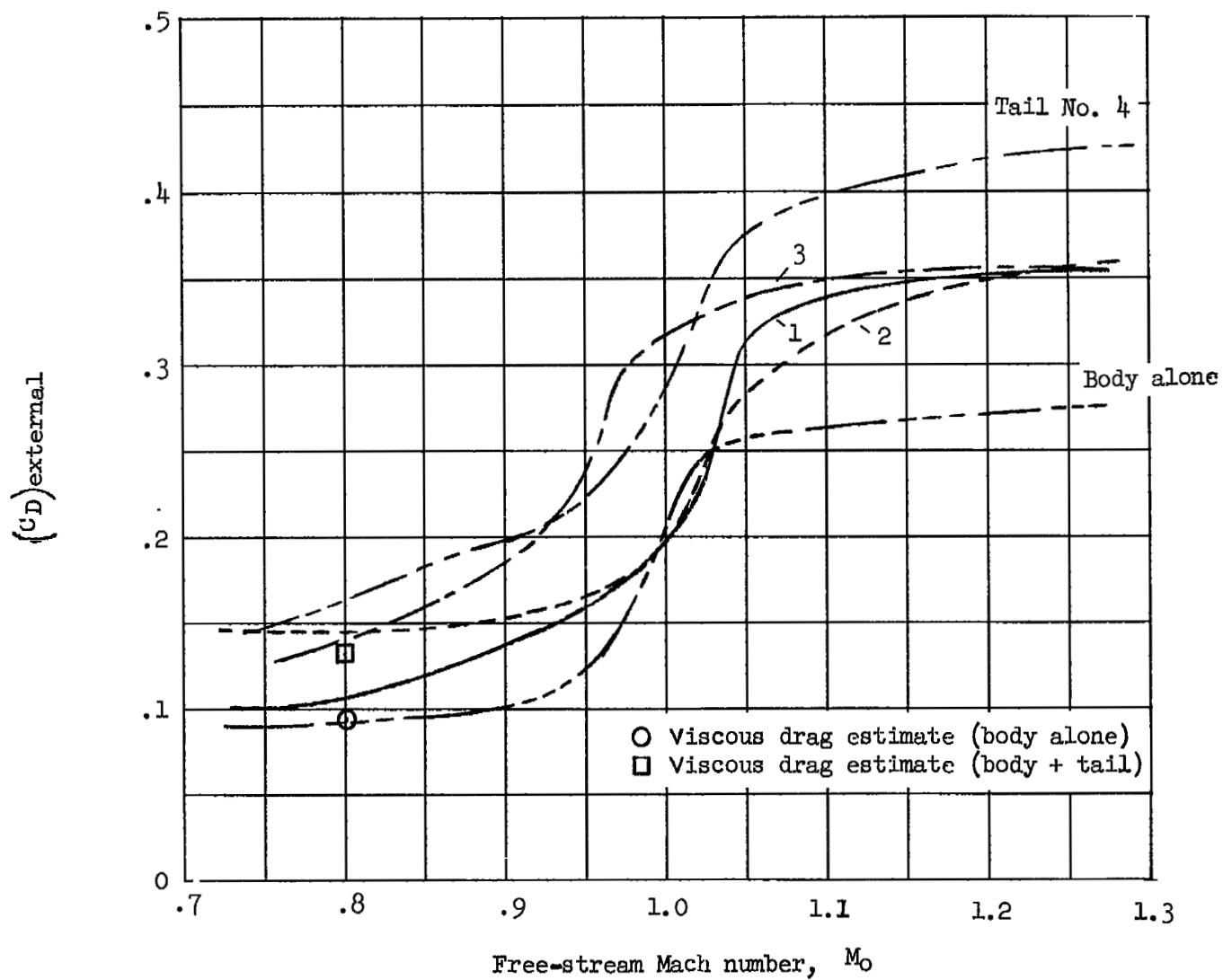


Figure 6.- Comparison of the external-drag-coefficient variation with Mach number of the various tail-body configurations and the body alone.

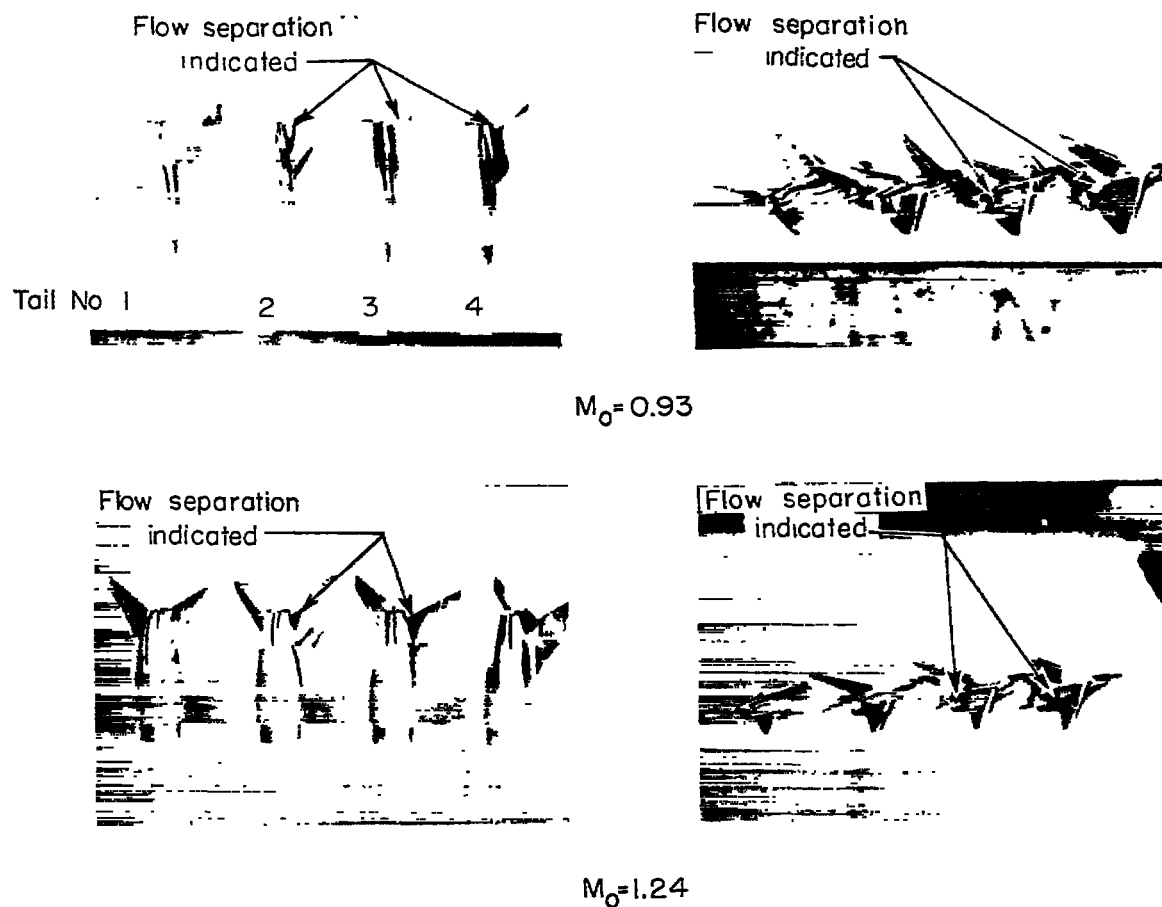
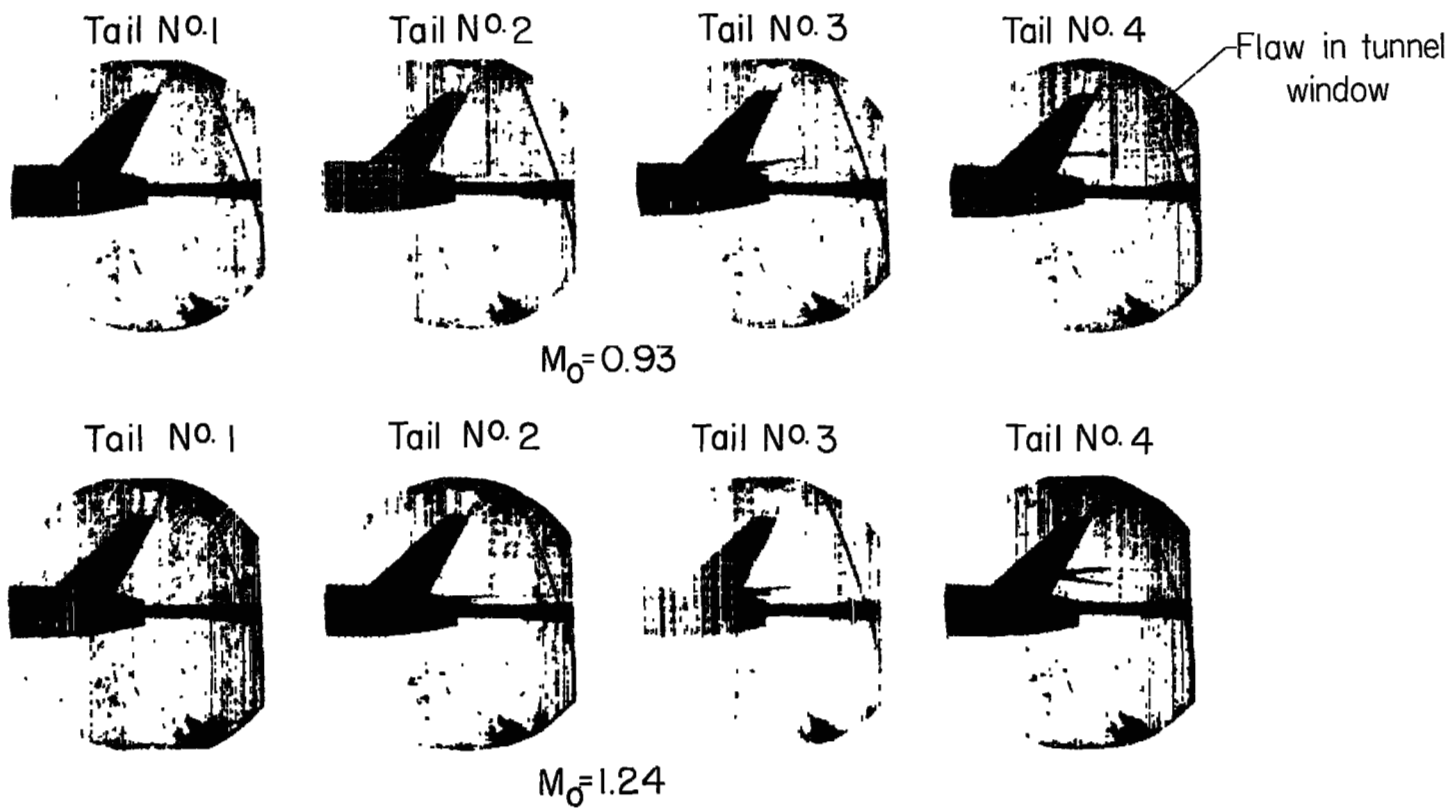


Figure 7.- Oil-flow patterns obtained with the various vertical locations of the horizontal tail for $M_0 = 0.93$ and 1.24 . L-93590



L-93589

Figure 8.- Side-view schlieren photographs of the tail-body combination with the horizontal tail at the various vertical locations for $M_0 = 0.93$ and 1.24.

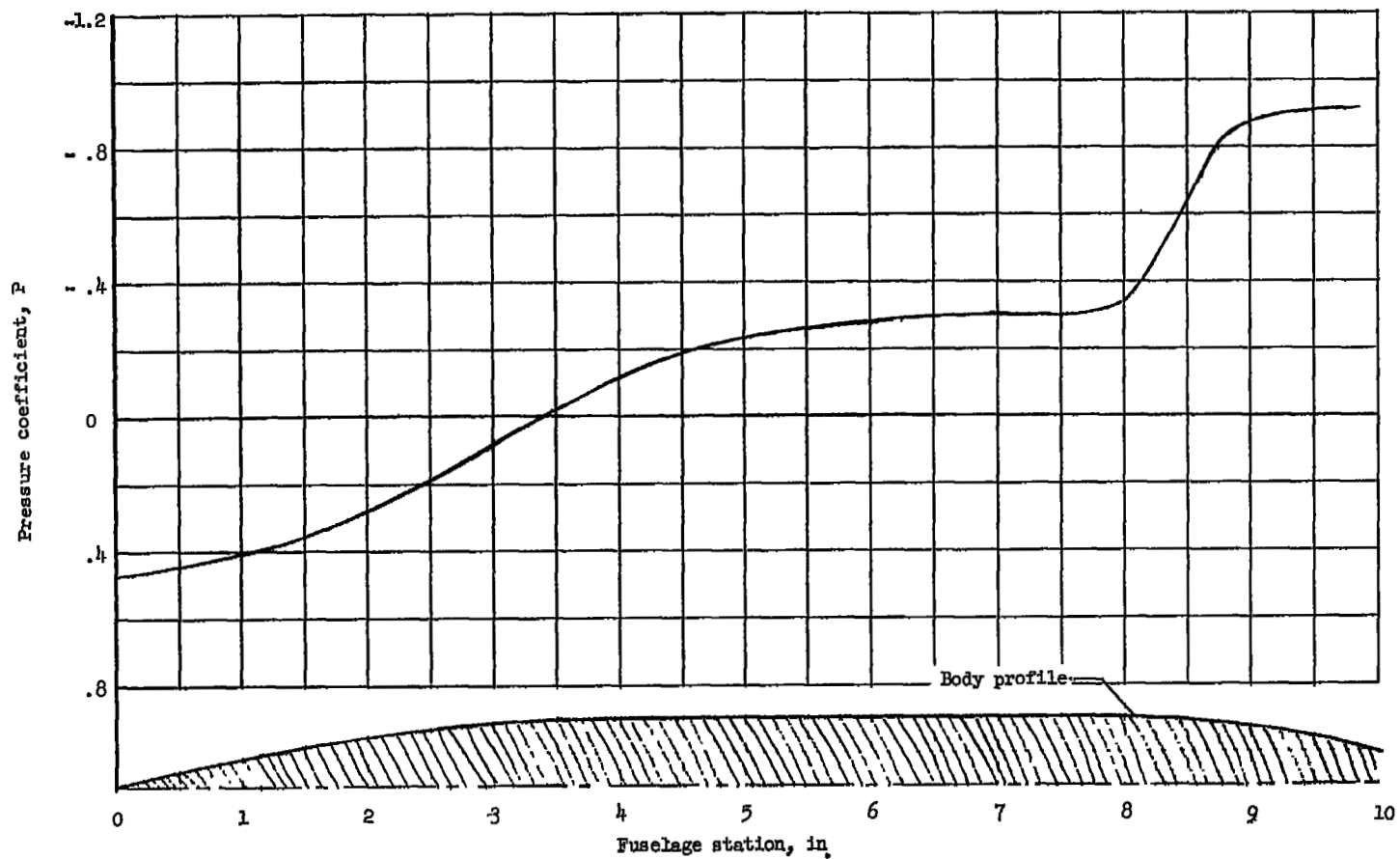


Figure 9.- Computed pressure distribution over the fuselage without the tail present. $\alpha = 0^\circ$; $M_0 = 1.2$.

NASA Technical Library
3 1176 01437 7411

[REDACTED]